Proceedings of the ASME 2012 6th International Conference on Energy Sustainability & 10th Fuel Cell Science, Engineering and Technology Conference
ESFuelCell2012
July 23-26, 2012, San Diego, CA, USA

ESFuelCell2012-91440

THERMAL MANAGEMENT OF AN AIR-COOLED PEM FUEL CELL: CELL LEVEL SIMULATION

M. Andisheh Tadbir
Mechatronic Systems Engineering
Simon Fraser University
BC,Canada
mandishe@sfu.ca

S. Shahsavari
Mechatronic Systems Engineering
Simon Fraser University
BC, Canada
sshahsav@sfu.ca

M. Bahrami
Mechatronic Systems Engineering
Simon Fraser University
BC, Canada
mbahrami@sfu.ca

E. Kjeang
Mechatronic Systems Engineering
Simon Fraser University
BC, Canada
ekjeang@sfu.ca

ABSTRACT

Air-cooled polymer electrolyte membrane (PEM) fuel cells have recently been the center of attention mainly because of the simplicity they bring into the fuel cell industry. Their main advantage is the elimination of balance-of-plant subsystems such as the liquid coolant loop, heat exchanger, compressor, and air humidifier which greatly reduces the complexity, parasitic power, and cost of the overall system. In air-cooled fuel cells, air is used as a combined oxidant and coolant. However, the net power output is limited by the heat rejection rate and the overall performance and durability are restricted by high temperature gradients during stack operation. An important initial step toward this goal is accurate knowledge of the temperature distribution in the stack in order to optimize heat removal by suitable thermal management strategies.

In the present study, a three dimensional numerical model is developed that can predict the temperature distribution in cell level with an acceptable accuracy. Using this methodology, the maximum temperature in the stack as well as temperature gradients, which are two essential operating parameters for air-cooled fuel cells, can be obtained. The model is validated using experimental data for the 1020ACS fuel cell stack from Ballard Power Systems. A parametric study is performed for bipolar plate thermal conductivity and overall thermal characteristics on the cell level to examine the effects of these parameters on the maximum stack temperature, temperature gradient in the cell, and overall heat rejection rate. Based on these results, recommendations are provided for improved thermal design of air-cooled fuel cells.

Keywords: PEM fuel cell, air cooling, numerical simulation, temperature map.

1. INTRODUCTION

Suitable thermal management is one of the most important issues in designing an efficient fuel cell. Each type of fuel cell can work reliably in a specific range of temperature [1]. The goal of thermal management is to keep the operating temperature within this range as well as reducing the temperature gradients in the cell. Low temperature gradients in the cell push the operating conditions toward the optimum design conditions. Moreover, uniform temperature distribution in the cell reduces the possibility of flooding and membrane dehydration.

Different methods can be used for thermal management of a PEM fuel cell depend on its application and its size [2]. In air-cooled PEM fuel cells which are mainly designed for auxiliary or backup power generation (1-4 kW), air has the role of oxidant and coolant at the same time. Many researches were conducted in the field of PEM fuel cell performance modeling and its thermal management [3-10]. But only few have focused their attention towards the thermal engineering aspect of the problem. A good review of different thermal management strategies for fuel cells is done by Faghri and Guo [1].

Among the CFD-based models that considered heat transfer, Yu and Jung [11] developed a two-dimensional numerical thermal model of a PEMFC and investigated a thermal management system for fuel cells with large active cell areas. Their fuel cell model was composed of sub-models for the water transport through the membrane electrolyte, the electrochemical reaction in the cathode catalyst layer and the temperature distribution within the fuel cell. Their heat transfer sub-model was focused on heat rejection from the fuel cell into the cooling water and included the conduction heat transfer inside the MEA and convective heat rejection from MEA to cooling water flow and gases. Pharoah and Burheim [12]

Copyright © 2012 by ASME

presented a two-dimensional thermal model and obtained temperature distributions in a PEMFC in the plane normal to the cathode flow direction. In their work, only conductive heat transfer was considered. A three-dimensional model was developed by Shimpalee and Dutta [13], which solved the energy equation to predict the temperature distribution inside a straight channel PEMFC. They analyzed the effect of heat produced by the electrochemical reactions on the fuel cell performance.

Adzakpa et al. [14] developed a three-dimensional dynamic model of a single cell to explain phenomena such as the cell humidity and voltage degradations. Their heat transfer model included the conduction and heat generation inside the fuel cell and the convection on the outer surface. Convective heat transfer inside the fuel cell was not considered in the model of [14]. A comprehensive three-dimensional model that included analysis of species, heat, and charge transport in a single-channel unit cell, was presented by Sinha and Wang [15]. They investigated the performance of a PEMFC operating at high temperature. In their thermal model, a constant temperature condition was applied on all the external boundaries of the fuel cell.

Ju et al. [16] presented a three-dimensional, thermal model coupled with electrochemical and mass transport models in order to study thermal and water management in PEMFCs. Their numerical simulation shows that the thermal effect on PEMFC becomes more critical at higher current density and/or lower gas diffusion layer thermal conductivity.

Our group recently developed a computational thermal model of the central cathode channel in an air-cooled fuel cell system [17]. [17] model can predict the maximum temperature in the air-cooled stack accurately. Moreover, effects of different parameters such as the in-plane and through-plane thermal conductivities of GDL and bipolare plate, and the inlet flow rate on the maximum temperature were studied. The model was however limited to analysis of a single cathode channel and was not able to predict temperature gradient in the whole cell. In order to improve the model and be able to obtain the temperature gradient in the cell, it is necessary to expand the computational domain to the cell level and include heat dissipation from the side walls. In the present investigation, a three-dimensional simulation of a complete single cell of an air-cooled PEMFC is performed numerically. The model is appropriately validated with experimental data and utilized to predict maximum temperature, temperature distribution, and temperature gradients on the cell level

2. MODEL DESCRIPTION

2.1. Model geometry and assumptions

Shown in Figure 1 is the Ballard 1020ACS fuel cell which has an open cathode which provides air to the stack both as a coolant and as an oxidant. To simplify the model and reduce the computational cost, an equivalent solid layer is assumed for modeling the heat transfer in the anode region. Convective heat transfer in the anode channels is neglected due to the comparatively low hydrogen flow rates.

Figure 1. Two Ballard 1020ACS air-cooled fuel cell stacks [18].

Based on orthotropic thermal conductivity of bipolar plate (60 W/mK in in-plane direction and 20 W/mK in through-plane direction) and also the thermal conductivity of hydrogen (0.18 W/mK), it is possible to estimate the effective thermal conductivity of the aforementioned equivalent solid layer by considering the corresponding thermal resistance network in each direction.

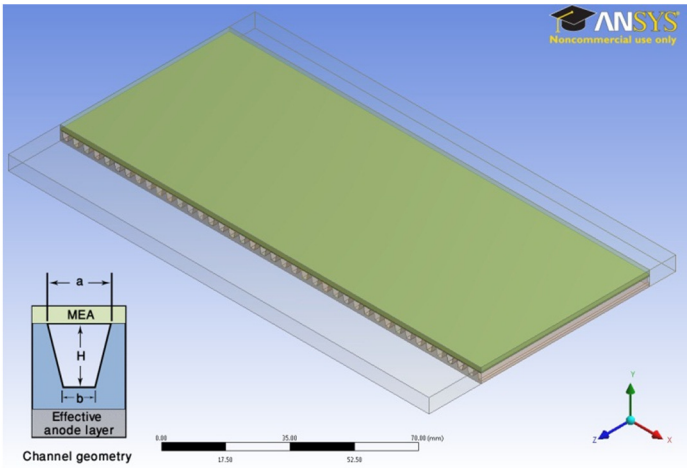

Figure 2. Schematic view of the half-cell bipolar plate used for baseline simulation.

A major challenge in fuel cell modeling is the highly coupled nature of different phenomena, length scales, and parameters. However, the art of engineering is to do some simplifications in order to decouple these phenomena by making reasonable assumptions. Since the main purpose of this work is to evaluate the thermal characteristics of the stack, the energy equation is decoupled from electrochemical equations. Instead, heat generation is calculated from experimental data. Moreover, flow in porous membrane, catalyst layers and GDLs (MEA) is not considered in this model. Similar to the procedure used for obtaining the effective thermal conductivity for the equivalent anode solid layer, effective thermal conductivity for the MEA is also calculated.

Copyright © 2012 by ASME

2.2. Governing equations

As stated earlier in section 2.1, in this model the energy equation is decoupled from the electrochemical equations and performance characteristics of the stack are inserted into the model from experimental data. Hence, the governing equations for this problem are the conservations of mass, momentum and energy, as well as ideal gas law. These equations are shown in (1)-(4).

$$\rho \nabla . \vec{V} = 0 \tag{1}$$

$$\rho \vec{V} . \nabla \vec{V} = -\nabla p + \nabla . (\mu \nabla \vec{V}) \tag{2}$$

$$\rho \nabla . \left(c_p \vec{V} T\right) = \nabla . (k \nabla T) + S_t \tag{3}$$

$$\rho = p_{atm}/(RT) \tag{4}$$

The last term in Eq. (3), S_t, is the source term due to heat generation in the cell which is only non-zero in the MEA and can be obtained from Eq. (5).

$$S_t = \frac{(E_{th} - V_{cell})I}{\forall} \tag{5}$$

where E_{th} is the thermodynamic potential which is the maximum voltage that can be obtained from the fuel cell if the whole enthalpy of formation of the fuel (hydrogen) will be transformed into electrical energy [2]. Eq. (6) shows the relation for E_{th}.

$$E_{th} = -\frac{\Delta H}{nF} \tag{6}$$

Considering the lower heating value (LHV) of hydrogen at 25 ℃ and 100 kPa, -241,826 kJ/mol, E_{th} will be equal to 1.253 *V*. Also, V_{cell} in Eq. (5), is the cell voltage, the value of which is obtained from experimental data for at given operating conditions, *I* is the electrical current, and $\forall$ is the volume of MEA. It should be noted that in this investigation, it is assumed that heat generation in the MEA is uniformly distributed throughout the MEA.

2.2. Boundary conditions

The cell which is considered in the present model is the central cell of a complete air-cooled stack. Since the number of cells in these fuel cells is large (more than 28 for each stack), in our model we consider periodic boundary conditions for the upper and lower boundaries. To be able to capture the heat transfer from the bipolar plate sides at the cell inlet and outlet zones, air plenums are considered at the entrance and exit regions of the cell.

In the present case air enters cathode channels as a result of suction provided by a fan at the outlet region. The boundary condition for the inlet of the entrance plenum is therefore assumed to be the atmospheric pressure, while for the outlet boundary of the exit plenum velocity is set since the flow rate from the fan is known.

Due to the symmetric nature of the problem, only half of the cell is modeled. The right side of the computational domain shown in Figure 2 is the symmetry boundary condition. For the lateral walls (left side of the computational domain in Figure 2) natural convection with a constant convective heat transfer coefficient is assumed. The value of convective heat transfer coefficient is obtained by calculating the local Nusselt number for a vertical flat plate of length equal to the height of the stack. Eq. (7) which is obtained from [19] shows the corresponding relation to calculate Nusselt number. Convective heat transfer coefficient for this problem is then computed to be 5 W/m^2K.

$$Nu_x = \left(\frac{Gr_x}{4}\right)^{1/4} g(\mathrm{Pr}) \tag{7}$$

2.3. Solution method

The model geometry is first meshed by the ANSYS meshing software with a structured grid. The governing equations with the aforementioned boundary conditions are then solved using ANSYS Fluent software. SIMPLE algorithm is used for solving the pressure-velocity coupling in the fluid zones. Power-law scheme is used as discretization method of momentum and energy equations and for pressure equation the standard method is used.

3. RESULTS AND DISCUSSION

3.1. Grid independency study

In the present study four different grid sizes are considered to check the grid dependency of results. Figure 3 depicts the value of maximum temperature calculated for the operating conditions of test #1 (details of which are described in Table 1). As illustrated in this figure, by increasing the number of computational nodes from 5.5 million to 11 million the difference between the calculated values is only 0.1℃, while the required time for convergence (with an Intel® Core™ i7 3.0GHz processor PC in parallel computation using 4 parallel nodes and 12GB of RAM) will increase from around 4 hours to 4 days. Hence, in our simulations we used the mesh with 5.5 million numbers of nodes.

3.2. Model validation

In order to validate the model, numerical results obtained from the present model are compared to experimental data measured at Ballard labs. The temperature distribution along the cell length for the experimental data and numerical result for two different test cases are shown in Figure 4. Operating conditions for these two cases are tabulated in Table 1.

Copyright © 2012 by ASME

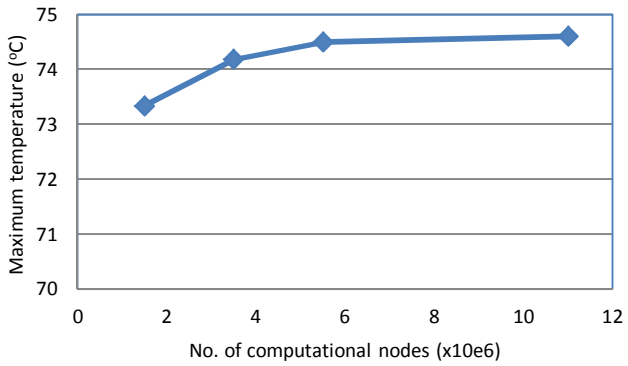

Figure 3. Maximum temperature in the computational domain with different grid sizes.

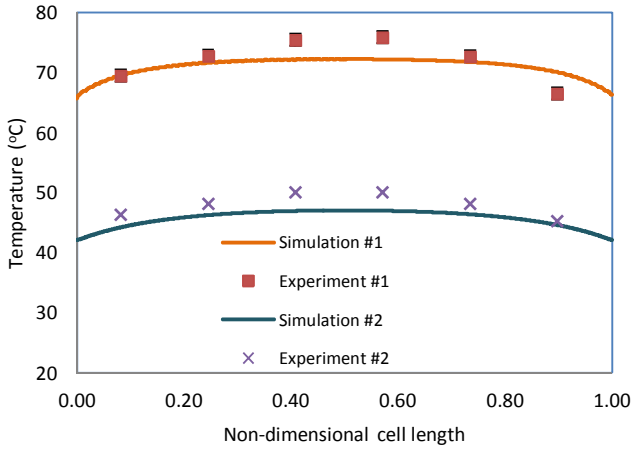

Figure 4. Comparison between experimental data and the present modeling results.

As shown in Figure 4, numerical results have a good agreement with experimental data. Maximum deviation of the numerical results from the experimental data is less than 6%, which is observed at the center of the domain. We expect this difference to be caused by the decoupling of the energy equation from the electrochemical reactions, i.e., the assumption of uniform heat generation. This assumption is however important at this stage to reduce the computational cost and resolve the entire cell domain. Hence, the model can predict temperature distribution in the cell level with an acceptable accuracy.

Table 1. Stack operating conditions used for validation.

Test #1	
Stack current	87.0 A
Cell voltage	0.569 V
Air flow rate	86.7 lpm
Ambient temperature	21 ℃
Test #2	
Stack current	29.0 A
Cell voltage	0.78 V
Air flow rate	26 lpm
Ambient temperature	20 ℃

3.3 Baseline study

Using the validated model, it is now possible to consider a reference case and investigate its thermal behavior under different conditions. Cell dimensions and flow conditions for the reference case are listed in Table 2.

Table 2. Cell dimensions* and operating conditions for the reference case.

Parameter	Value
Stack current	50.0 A
Cell voltage	0.6 V
Air flow rate	80 lpm
Ambient temperature	20 ℃
MEA thickness	0.45 mm
Cathode channel height (H)	2.5 mm
Trapezoidal base (a, b)	2.5, 1.5 mm
Effective anode layer thickness	1.0 mm
Rib width	1.5 mm
Cathode channel length	60 mm
No. of cathode channels	80

*Channel dimensions are based on the parameters shown in Figure 2.

Shown in Figure 5 is the temperature distribution for the reference case. The maximum temperature is found to occur near the exit of the central channel. Although the previous work done by our group [17] could predict the maximum temperature in the stack accurately, it is necessary to model the whole cell to see the temperature variations in it. By looking at Figure 4 we can see a moderate temperature gradient exists along the cell length. In the previous model [17], since only one channel was considered, variations of temperature in the x-direction were not observable and the maximum temperature may have been overestimated by neglecting heat transfer to adjacent channels. In the present simulation however, three-dimensional heat transfer is captured in the entire cell.

For the reference case, minimum and maximum temperatures in the bipolar plate are obtained to be 38.8 ℃ and 49 ℃, respectively. Hence, the temperature variation in the cell is 10.2 ℃. Almost the whole heat generation in the cell is transferred via forced convection in the channels and free

Copyright © 2012 by ASME

convection from the side walls has relatively small contribution to the overall heat dissipation. The overall heat transfer coefficient for this case, which can be calculated from Eq. (8), is 1.62 W/K for each cell. In Eq. (8), $\dot{Q}_{tot}$ is the total heat generation in the cell and ΔT is the difference between inlet and outlet mean temperatures.

$$UA = \frac{\dot{Q}_{tot}}{\Delta T} \tag{8}$$

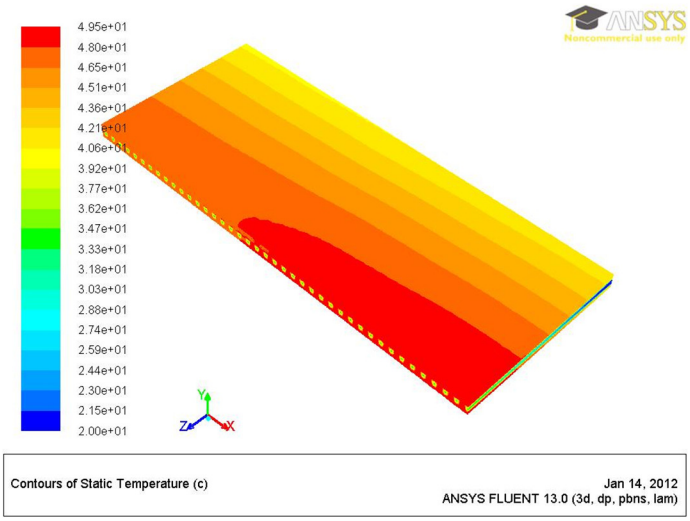

Figure 5. Temperature distribution in the half-cell for the reference case.

Pressure drop in the cell is also an important parameter which is under influence of channel geometry and flow rate. For the reference case, the pressure drop is computed to 44 Pa.

3.4. Effects of bipolar plate thermal conductivity

Thermal conductivity of bipolar plate plays an important role in the temperature distribution in the cell. It is anticipated that by increasing the bipolar plate thermal conductivity, we can get more uniform temperature in the cell. It is observed in [17] that the through-plane thermal conductivity of bipolar plate does not have a significant impact on temperature distribution (assuming that the in-plane thermal conductivity is fixed). Present simulation results also confirm that finding. Figure 6 shows the distribution of temperature along the central line of the cell for two different cases, namely for the through-plane thermal conductivities of 20 and 60 W/mK. No significant change in temperature distribution is seen for these two different thermal conductivities. However, in this stage it is not possible to conclude that the through-plane thermal conductivity has no effect on temperature distribution in a complete air-cooled stack. In other words, it is not possible to see the effects of the through-plane thermal conductivity by considering only one cell with periodic boundary conditions. The effects of this parameter can be discussed more accurately and in more detail in our next work which will be the stack level modeling.

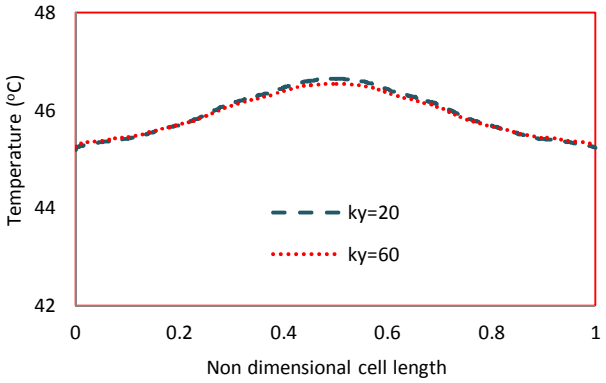

Figure 6. Temperature distribution along the *x*-direction at the centre of of the cell.

The in-plane thermal conductivity of the plate is found to be much more significant than the through-plane parameter. As shown in Figure 7, by increasing the in-plane thermal conductivity from 60 W/mK to 600 W/mK, the maximum temperature in the plate will decrease from 49.2 ℃ to 47.2 ℃. The maximum temperature difference in the plate (which is a good indicator of temperature gradients in the cell) will also decrease from 11 ℃ to 4.3 ℃. There is however no significant change in temperature gradients in the cell by increasing the in-plane thermal conductivity beyond 300 W/mK. It is worth to mention that in the previous model [17], we were not able to calculate the maximum temperature difference in the cell. Since, the minimum cell temperature will occur at the cell sides. However, in the present study it can be accurately computed. These high thermal conductivities are reachable by using new materials such as pyrolytic graphite sheets [20,21].

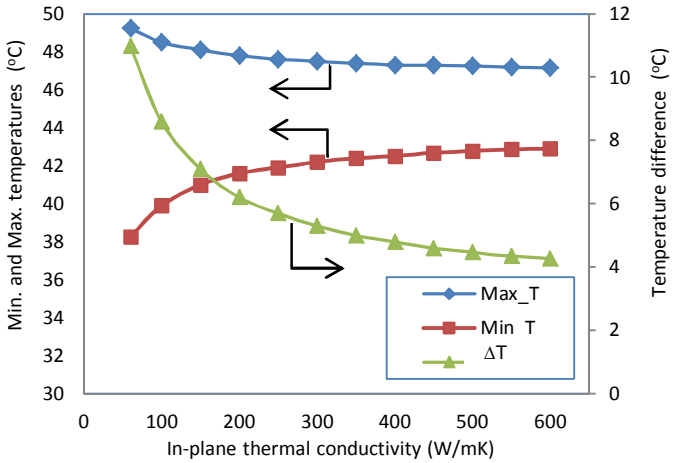

Figure 7. Variations of minimum, maximum and temperature difference in bipolar plate with in-plane bipolar plate thermal conductivity.

Copyright © 2012 by ASME

4. CONCLUSION

In the present work, a three dimensional simulation of a complete single cell from an air-cooled fuel cell stack is presented. In this model, in order to reduce the complexity of model while still capturing the thermal behavior of the cell with an acceptably low computational cost, electrochemical reactions in the fuel cell is not considered and the heat generation is calculated based on experimental data. Results from this model are successfully validated against measured temperature distributions for the Ballard 1020ACS air-cooled stack. It is noteworthy that the model can accurately predict temperature distribution in different points of the cell with errors lower than 6%.

Baseline simulations show that the maximum temperature occurs at the central channel and the maximum temperature difference in the bipolar plate is calculated to 10.2 ℃. Moreover, it is observed that most of the heat generated in the cell is transferred via forced convection inside the cathode channels and natural convection from the side wall has limited effect on the overall heat rejection.

Effects of in-plane thermal conductivity of bipolar plate are also studied. By increasing this parameter from 60 W/mK to 300 W/mK, the maximum temperature difference in the cell (for the case under investigation) is reduced by almost 6 ℃ (from 11 to 5.3 ℃). Beyond 300 W/mK the effects are not significant. Hence, it is favorable to use materials with in-plane thermal conductivities of near 300 W/mK to reduce temperature gradients in the cell.

ACKNOWLEDGMENTS

We would like to acknowledge Ballard Power Systems and Natural Sciences and Engineering Research Council of Canada, NSERC, for supporting this research.

NOMENCLATURE

a, b	Bases for trapezoidal channel cross section
c_p	Constant pressure specific heat (J/mol.K)
E_{th}	Thermodynamic potential (V)
F	Faraday's constant (96,485 C/mol)
h	Convective heat transfer coefficient (W/m^{2}K)
H	Cathode channel height (m)
I	Electrical current (A)
k_x, k_y, k_z	Thermal conductivity in x, y, or z direction (W/mK)
n	Equivalent electrons per mole of reactant (n=2)
p	Pressure (Pa)
$\dot{Q}_{tot}$	Total heat generation (W)
S_t	Energy equation source term (W/m^3)
UA	Overall heat transfer coefficient (W/K)
V_{cell}	Cell voltage (V)
$\vec{V}$	Velocity vector (m/s)
$\forall$	MEA volume (m^3)

Greek symbols

ΔH	Lower heating value of hydrogen (kJ/mol)
ρ	Density (kg/m^3)
μ	Fluid viscosity (Ns/m^2)

REFERENCES

[1]. A. Faghri, Z. Guo, Challenges and opportunities of thermal management issues related to fuel cell technology and modeling, International Journal of Heat and Mass Transfer, 48(19-20) (2005) 3891–3920.

[2]. J. Larminie, A. Dicks, Fuel Cell Systems Explained, John Wiley, 2002.

[3]. X. Yu, B. Zhou, A. Sobiesiak, Water and thermal management for Ballard PEM fuel cell stack, Journal of Power Sources, 147(2005) 184–195.

[4]. S. Pandiyan, K. Jayakumar, N. Rajalakshmi , K.S. Dhathathreyan, Thermal and electrical energy management in a PEMFC stack – An analytical approach, International Journal of Heat and Mass Transfer, 51 (2008) 469–473.

[5]. J.E. Dawes, N.S. Hanspal, O.A. Family, A.Turan, Three-dimensional CFD modeling of PEM fuel cells: An investigation into the effects of water flooding, Chemical Engineering Science 64 (2009) 2781–2794.

[6]. M.S. Al-Baghdadi, H.A.K.S. Al-Janabi, Modeling optimizes PEM fuel cell performance using three-dimensional multi-phase computational fluid dynamics model, Energy Conversion and Management 48 (2007) 3102–3119.

[7]. L.S. Martins, J.E.F.C. Gardolinski, J.V.C. Vargas, J.C. Ordonez, S.C. Amico, M.M.C. Forte, The experimental validation of a simplified PEMFC simulation model for design and optimization purposes, Applied Thermal Engineering 29 (2009) 3036–3048.

[8]. A.P. Sasmito, K.W. Lum, E. Birgersson, A.S. Mujumdar, Computational study of forced air-convection in open-cathode polymer electrolyte fuel cell stacks, Journal of Power Sources 195 (2010) 5550–5563.

[9]. A. Kopanidis, A. Theodorakakos, M. Gavaises, D. Bouris, Pore scale 3D modelling of heat and mass transfer in the gas diffusion layer and cathode channel of a PEM fuel cell, International Journal of Thermal Sciences 50 (2011) 456–467.

[10]. K.S. Choi, H.M. Kim, S.M. Moon, Numerical studies on the geometrical characterization of serpentine flow-field for efficient PEMFC, International Journal of Hydrogen Energy 36 (2011) 1613–1627.

[11]. S. Yu, D. Jung, Thermal management strategy for a proton exchange membrane fuel cell system with a large active cell area, Renewable Energy 33 (2008) 2540–2548.

[12]. J.G. Pharoah, O.S. Burheim, On the temperature distribution in polymer electrolyte fuel cells, Journal of Power Sources (2010) 195 5235–5245.

[13]. S. Shimpalee, S. Dutta, Numerical prediction of temperature distribution in PEM fuel cells, Numerical Heat Transfer Part A (2000) 38 111-128.

Copyright © 2012 by ASME

[14]. K.P. Adzakpa, J. Ramousse, Y. Dubé, H. Akremi, K. Agbossou, M. Dostie, A. Poulin, M. Fournier, Transient air cooling thermal modeling of a PEM fuel cell, Journal of Power Sources (2008) 179 164–176.
[15]. P.K. Sinha, C.Y. Wang, U. Beuscher, Transport Phenomena in Elevated Temperature PEM Fuel Cells, Journal of The Electrochemical Society (2007) 154 B106–B116.
[16]. H. Ju, H. Meng, C.Y. Wang, A single-phase, non-isothermal model for PEM fuel cells, International Journal of Heat and Mass Transfer (2005) 48 1303–1315.
[17]. S. Shahsavari, E. Kjeang and M. Bahrami, Computational analysis of heat transfer in air-cooled fuel cells, ASME 9th Fuel Cell Conf., Aug. 7-10, 2011, Washington, DC, USA, Paper No. ESFuelCell2011-54265.
[18]. Ballard Power Systems' web site: http://www.ballard.com.
[19]. F.P. Incropera, D.P. Dweitt, T.L. Bergman, A.S. Lavine, Fundamentals of Heat and Mass Transfer, 6th Ed, John Wiley & Sons, 2006.
[20]. C.Y. Wen, Y.S. Lin, C.H. Lu, Performance of a proton exchange membrane fuel cell stack with thermally conductive pyrolytic graphite sheets for thermal management, Journal of Power Sources 189 (2009) 1100–1105.
[21]. C.Y. Wen, Y.S. Lin, C.H. Lu, T.W. Luo, Thermal management of a proton exchange membrane fuel cell stack with pyrolytic graphite sheets and fans combined, International Journal of Hydrogen Energy 36 (2011) 6082–6089.

Copyright © 2012 by ASME